JOINT INSTITUTE FOR NUCLEAR RESEARCH
Veksler and Baldin laboratory of High Energy Physics

Final Report of INTEREST program

Event Shape Variables to study Heavy Ion Collisions at MPD

Supervisor
Dr. Ivonne Maldonado
Student
Irving Gaspar
Universidad Autonoma Metropolitana

Wave 9. February 13th - March 26th, Dubna 2023

Abstract

In this project we present measurements of the event shape variables, sphericity and spherocity mainly, focusing on the characterization of charged particles, such as protons, pions, and kaons by means of 230,000 Bi+Bi collisions with an energy of 9.2 GeV in the center-of-mass frame. This collisions were produced by using the UrQMD event generator and utilizing the ROOT environment for the analysis. We considered cuts in pseudo-rapidity, $|\eta| < 1.3$ in order to avoid the presence of protons out of the validity range of the Time Projection Chamber at MPD. The distributions of sphericity and spherocity as functions of impact parameter, and the splitting of sphericity and spherocity into jetty and isotropic events for different types of centralities is also presented. Finally, the mean transverse momentum and multiplicity for charged particles as a function of different types of jetty and isotropic events for different types of centralities in sphericity and spherocity is also presented.

Introduction

The study of heavy ion collisions awakened the interest among the scientific community, specially in the high energy physics. As we know by the Quantum Cromo Dynamics, the nucleons have structure, that is, protons and neutrons are made of more fundamental particles called "quarks" [1]. The first time that the concept of quark was heard came from the development of the quark model, introduced by M. Gell-Man and G. Zweig in 1964 [2, 3]. Five years after the establishment of this model, deep inelastic scattering experiments were performed at the Stanford Linear Accelerator Center (SLAC for short) in 1968, where in a subsequent publication, one year later, the experiment collaborators showed that the proton are indeed made of point-like objects more fundamental than protons, contrary what is expected in those years [4, 5]. Such objects were after identified as "up" and "down" quarks, and more flavors were discovered in the following years; for instance, the charm quark was detected in two facilities independently, at SLAC, and at the Relativistic Hadron Ion Collider (RHIC) in 1974; the bottom quark was discovered independently by two research teams at Fermilab in 1977 [6], among other flavors known in the literature, such as strange and bottom quarks were found. The discovery of this point-like particles motivated R. Feynman to develop a model which describes this phenomena, this model is known in the literature as the "parton model" [7], which is useful in recent experiments. The study of collisions at high energy became relevant as new phenomena arose; for instance, there are certain collisions where the particles produced by hadronization have a preferred direction of propagation, this is known as jets. Those jets are defined as cascades of consecutive emissions of partons, caused by other partons (protons and neutrons) involved in hard processes. Another interesting case is the discovery of the quark gluon plasma, which under certain conditioons presents vortical efects [8]. In order to study and characterize the different type of phenomena in heavy ion collisions, it is customary to focus in the geometrical properties of the energy flow for this processes, and that is how the concept of event shape variables arose. Event shape variables describe the patterns, correlations, and showed to be a indirect probe of multi-jet topologies [9],

that is, different branches where different cascades of particles are produced. These variables are widely used in different experiments and simulations, from the measurement of the coupling constant and the test for the asymptotic freedom up to the search for physics beyond the Standard Model [9]. The event shape variables we will focus are spherocity and sphericity, but it is worth mentioning the existence of other variables, such as aplanarity A [9], the transverse thrust $T_{\perp}$, the minor transverse thrust component $T_{m,\perp}$, the complement of the transverse thrust, and so on [10]. As this kind of processes occurs in a short period of time, the only way to characterize is by means of reconstruction, which can be achieved through calculations using the final state of the particles produced after the collisions, consequence of the deconfinament in the collision, in other words, the boundaries that maintain quarks together vanishes, and hadronization, that is, the restoration of those boundaries. In the case of the event shape variables taken into account in this project, they will depend on the transversal momentum detected. As one can expect, the heavy ion collisions have ranges of energy where different phenomena occurs, in view of that fact, different theoretical models has been developed to characterize their dynamics, going from effective theories in QCD and Lattice QCD, up to transport models, such as the Ultra relativistic Quantum Molecular Dynamics (UrQMD) [11, 12]. In addition, different facilities are being built in order to cover the energy range where is not easily reached by other facilities; for instance, the novel Russian facility located at NICA, the MPD experiment [13]. This project is organized as follows. In the Sec. I we mentioned some of the goals of this project, in Sec. II we established the scope of our work, the difficulties we had, and the parameters we took. Sec. III is dedicated to explain the methodology followed, passing through a brief introduction of the MPD experiment, its purposes and infrastructure; therefore, we will explain the most important concepts, such as the UrQMD model, the kinematic variables, and the event shape variables, sphericity and spherocity, specifically. In Sec. IV we present our results. Finally, in Sec V. the conclusions are presented, with the most important insights obtained from the data, and further discussion.

1 Project Goals

The main goals of this project are:

1. To develop a software to measure event shape variables within MPDRoot framework.
2. To calculate event shape variables as a function of centrality in heavy ion collisions at NICA energies.
3. To determine if the event structure variables help to differentiate between the most central and most peripheral events in Ultra relativistic Quantum Molecular Dynamics (UrQMD) [11] experiment.

2 Scope of the work

In the present work 230,000 events have been analyzed based on ion-ion collisions at NICA energies provided by UrQMD event generator. Nucleus of Bismuth with a charge $Z = 83$ and an atomuc number of $A = 209$ were used. The range of the impact parameter for the collisions goes from 0 to 16 femtometers (fm). The energy of the beam considered in this events is considered by the center-of-mass, which its values is $\sqrt{s_{NN}} = 9.2\ GeV$ where s is one of the three Mandelstam variables, important in the scattering processes in a Lorentz-invariant frame. Finally, the output particles given by the UrQMD event generator were lambdas Λ and anti-lambdas $\bar{\Lambda}$ particles, kaons, pions, and protons. The reason why we chose 9.2 GeV as energy is because we can compare this result with the data obtained at RHIC-STAR through Au+Au collisions with the value of 11 GeV in the center of mass frame.

3 Methodology

In this section we start by talking about the MPD experiment, describing the type of phenomena that motivated its construction and the main subsystems present in the overall MPD setup. Afterwards, we proceed with a brief introduction of the event generator based on the UrQMD model. Then, we proceed to define the kinematic variables that serve as observables in heavy ion collisions. Finally, define the shape variables of interest, that are, the transversal sphericity and spherocity before performing our detailed analysis.

3.1 MPD experiment

The Multi-Purpose Detector, or MPD for short, is an apparatus designed as a 4π spectrometer where we can measure the variation of physical characteristics over given ranges, for instance the transverse momentum. This spectrometer is capable of detecting charge hadrons, electrons, and protons in heavy ion collisions at high luminosity in the energy range reached in experiments at the Nuclotron-based Ion Collider fAcility, or NICA for short. The main goal of this experiment is the research for new phenomena in the barionic-rich region of the Quantum Chromo Dynamics (QCD) phase diagram by virtue of heavy nuclei collisions in the energy range of $4\ GeV \leq \sqrt{s_{NN}} \leq 11\ GeV$, specifically. In order to satisfy this purpose, the detector will comprise two novel systems, a precise 3-D tracking system and a high-performance particle identification systems supported by time-of-flight measurements and calorimetry. In previous years many facilities have obtained measurements above several hundreds of MeV per nucleon (AMeV) by virtue of heavy ion collisions in three main energy regions. First, at about 1AGeV at BEVALAC in Berkeley or at the Super Ion Synchrotron (SIS) at GSI-Darmstadt. Second, the energy regime ranging from 2 AGeV to 15 AGeV at the Alternating Gradient Synchrotron (AGS) in Brookhaven. Third, the energy range from 40 AGeV to 200 AGeV reached in the Super Proton Synchrotron at CERN. Finally, important efforts achieved to working on energy regimes greater than $\sqrt{s} \approx 200$ AGeV and $\sqrt{s} \approx 6$ ATeV, now available in the Relativistic Heavy Ion Collider at Brookhaven and in

LHC at CERN, respectively. In conclusion, this novel experimental program will cover the void of the energy scale not yet explored, expecting that bring us important insights into hadron dynamics and multi particle production in a high baryon density frame.

As a motivation, this ambitious project covers a wide number of interesting phenomena. Firs of all, the interests for this project are closely related to results provided by the Lattice Quantum Chromo Dynamics (LQCD) calculations regarding to the pseudo-critical temperature from the confined/broken chiral symmetry phase to the deconfined/partially restored chirally symmetry phase for the case of vanishing baryon chemical potential $\mu_B \approx 0$ [14, 15]. But, different effective model calculations [16–18] suggest that for low temperatures and high baryon chemical potential, the transition from common hadron matter phase to a phase where chiral symmetry is restored is of the first order. But, whether as the temperature increases, the end of this first-order phase transition line in the T vs μ_B plane should happen at a Critical End Point (CEP), but its existence is not established yet [19] since its location in models that predict its existence is widely spread over the phase diagram [20]. In this sense, the MPD experiment is a promising tool for determining this CEP owing to calculations within the thermal model, where it is indicated that the highest baryon density is achieved in the NICA energy range [21]. Another example of MPD impact relies in the astrophysics field where recent model calculations revealed that in a neutron star merger, the nuclear matter reaches densities and temperatures comparable to those occurring in heavy ion collisions in the NICA energy range [22, 23], that is, heavy ion collisions at NICA and neutron star mergers share similar regions of the QCD phase diagram. In view of the previous fact, the MPD could contribute in the study of neutron star merger by obtaining data from laboratory experiments [24]. It is important to highlight that if the observations of neutron stars and their merges could reveal the existence of a first order phase transition, this would necessary imply the existence of a critical end point in the QCD phase diagram, further details can be checked in [25, 26]. The last set of fascinating phenomena that MPD is suited to study includes vortical effects [8, 27–30] and magnetic fields [31, 32] produced in non-central heavy ion collisions; the color superconducting phase with large pairing gaps [33–35] for quark matter at low temperatures and its relation with the changes in the chiral and superconducting phase transition at low temperatures into a crossover, where could involve the existence of a second critical end-point or its absence [36]; the search for light nuclei formation to characterize its influence on the Equation of State at high baryon densities [37, 38], and the production of isospin imbalanced matter, extensively explained in [39–43].

The MPD setup consists mainly of two stages, but in this part we will focus just on the first stage. An schematic representation of the overall set-up of MPD is shown in the Fig. 1. The fist thing to notice is the cylindrical geometry for the central barrel components. The first two components are the Time Projection Chamber (TPC), which is surrounded by the Time of Flight Detector (TOF). The TPC is known as the main tracker of the MPD central barrel, one TPC purpose is to make 3-D precise tracking of charged particles and momentum measurements in

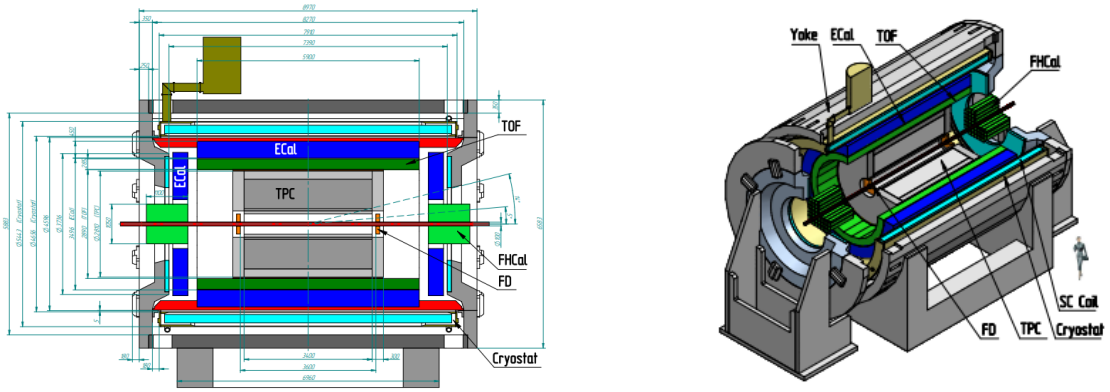

(a) This is an schematic representation of the MPD subsystems in the stage one in a cross-section view.

(b) Three-dimensional representation of the overall MPD subsystems in the stage one

Figure 1: Schematic representations for the overall MPD subsystems in 3-D and cross-sectional views.

the transverse plane, it identify the charged particles by measuring their ionization energy losses by means of the gas inside the detector. The second component is the Time of Flight Detector, or TOF for short. The TOF detector was developed to identify charged hadrons in an intermediate momentum range, it also gives time and coordinate measurements with high accuracy, approximately 80 picoseconds and 0.5 centimeters, in its default configuration consists of a barrel with 14 plate sectors. Afterwards, between the TOF and the MPD magnet we found the Electromagnetic Calorimeter (ECal), used mainly in the measurement of spatial position and total deposited energy of electromagnetic cascades induced by electrons and photons involved in the ion collisions. The orange small plates within the TPC barrel, see Fig. 1a, are known as the Fast Forward Detector (FFD), which purpose is to provide fast triggering of A+A collisions and sets the start-time pulse generation for the Time of Flight detector with 50 picoseconds or better of resolution, it also has the function for the adjustment of collisions in the center of MPD chamber, where the collisions occurs. In the external part, near to the Magnet end-caps one finds the Forward Hadronic Calorimeter (FHCal), and its function relies in the determination of the collision centrality and the orientation of the reaction plane in collective flow. Finally, we have the essential component of the overall MPD subsytems, the solenoid magnet with a superconducting NbTi coil and a steel flux return yoke, this magnet provides a high homogeneous magnetic field, up to 0.57 T, uniform along the beam direction. Further specifications for each component here presented, and additional description about the other hardware and software components can be found in [13].

3.2 UrQMD model

The Ultra relativistic Quantum Molecular Dynamics is a microscopic transport model where describes the individual hadron-hadron collsions in the energy range from about 1 AGeV at SchwerIonenSynchroton (SIS) at GSI-Darmstadt in Germany

to $\sqrt{s} \approx 200GeV$ at Relativistic Hadron Ion Collider in Brookhaven. This transport model is based on the covariant propagation of all the hadrons moving through classical trajectories in combination with stochastic binary scatterings, color string formation and resonance decay that appear when the quark and gluon degrees of freedom cannot be neglected. UrQMD models represents a Monte Carlo solution [11] of a enormous set of coupled partial integro-differential equations for the time evolution of our system of various phase space densities $f_i(x,p)$ of particle species i, which for a non-relativistic fashion assumes the well known Boltzmann form:

$$\frac{df_i(x,p)}{dt} \equiv \frac{\partial p}{\partial t}\frac{\partial f_i(x,p)}{\partial p} + \frac{\partial x}{\partial t}\frac{\partial f_i(x,p)}{\partial t} = Stf_i(x,p) \tag{1}$$

where x and p are the position and momentum of the particle, respectively; and $Stf_i(x,p)$ describes the collision (or rather source-) term of these particles species, which are connected to any other particle species f_k. In these model we can implement potentials, such as Skyrme, Yukawa and Coulomb potentials. The potential allows to calculate the equation of state of the interacting many body system, as long as it is dominated by nucleons. Finally, the UrQMD models is used to study a wide variety of heavy ion effects, such as the creation of dense hadronic matter ah high temperatures, properties of nuclear matter, mesonic matter and its anti-matter counterpart, etc. A complete schema of the applicability of the Ultra relativistic Quantum Molecular Dynamics model to heavy-ion reactions can be found in [11, 12]. For the most curious reader, we recommend to read the use manual dedicated for the UrQMD event generator in order to deeply understand the framework there developed [44].

3.3 Kinematic Variables

In order to characterize the particles produced from a hadron-hadron collisions we need to set a coordinate plane, it is customary to define a cartesian momentum space where the incoming and otcoming particles happen. The incoming particles, described by ion beams, are restricted to move along the z-axis, and the momentum of each particle produced after the collision can be split in two components. The component parallel to the beam, that is, the longitudinal momentum $p_L = p_z$; and, the momentum perpendicular to the beam axis, or transverse momentum $p_T^2 = p_x^2 + p_y^2$. The transverse plane can be represented in a polar coordinate frame using the transverse momentum as the magnitude and the azimuthal scattering angle defined by ϕ as the polar angle. The main feature of this transverse plane is the Lorentz invariance, in other words, the transverse plane remains the same when we apply a boost in the longitudinal direction, since the beam particles move in a relativistic way. The previous feature will be important later when we consider shape variables, such as sphericity and spherocity. Once we have defined the transverse plane, it is needed to define another variable that describes the plane by the z-xis and another axes, x- or y-axis, and must satisfy the Lorentz invariance. The variable suitable for this purpose is known as pseudo-rapidity η defined in terms of the angle in the center-of-mass θ_{cm} as:

$$\eta = -\ln\left(\tan\frac{\theta_{cm}}{2}\right), \tag{2}$$

where θ_{cm} is the angle at which the particles are scattered with respect to the collision beam. In the literature, pseudo-rapidity is a particular case of a Lorentz invariant particle called rapidity y, defined as

$$y \equiv \tanh^{-1}(v_L) = \frac{1}{2}\ln\left(\frac{E + p_L}{E - p_L}\right), \tag{3}$$

where v_L is the velocity parallel to the beam. So, for particles with an enormous quantity of momentum $|\vec{p}| \gg m$, the previous expression reduces to,

$$\eta \equiv y \approx \frac{1}{2}\ln\left(\frac{|\vec{p}| + p_L}{|\vec{p}| - p_L}\right), \tag{4}$$

this limit case is known as the pseudo-rapidity.Further details for pseudo-rapidity and rapidity can be found in [45].

3.4 Event Shape Variables

First, in the literature is commonly said that the event shape variables are used to test QCD because they are collinear and infrared safe observables, that is, these variables do not change their value when an extra soft gluon is added or if a parton is split into two collinear partons [46]. It is also important to emphasize that at hadron colliders event shapes are defined in the transverse plane, that is, the plane perpendicular to the beam axis where bais from the longitudinal boost in the beam directions are prevented [47, 48], but some experiments include the component along the beam axis [9].

Sphericity In order to define the first event shape variable, the sphericity, it is customary to define the transverse momentum matrix $\mathbf{S}$ primary as

$$\mathbf{S} = \frac{1}{\sum_i p_{T,i}} \sum_i \frac{1}{p_{T,i}} \begin{pmatrix} p_{x,i}^2 & p_{x,i}p_{y,i} \\ p_{x,i}p_{y,i} & p_{y,i}^2 \end{pmatrix}, \tag{5}$$

where the variable $p_{T,i}$ is the transverse momentum of the i-th particle, and the terms $p_{x,i}$ and $p_{y,i}$ are the components along the x, y plane, respectively. It is necessary to emphasize that we should diagonalize the matrix first. Therefore, the transverse sphericity denoted as S_T is defined in terms of the eigenvalues, $\lambda_1 > \lambda_2$ [9, 10] as

$$S_T \equiv \frac{2\lambda_2}{\lambda_1 + \lambda_2} \tag{6}$$

Another way to compute the the sphericity can be achieved by the "flow tensor" [49] defined as

$$F_{ij} = \sum_k^N \frac{p_i^{(k)} p_j^{(k)}}{2m_k} \tag{7}$$

in each event. Where its eigenvalues t_i are normalized via $q_i = t_i^2 / \sum_{i=1}^3 t_i^2$ allowing the calculation of the sphericity using $S_T = \frac{3}{2}(1 - q_3)$, the complete approach can be

found in [50]. Results have showed that all shape observables extracted form this flow tensor (such as sphericity, S_T) depend strongly on the number of particles [51, 52]. The values for sphericity lies from 0 to 1, where one can classify the lowest value 0 as "the jetty limit" and the highest value 1 as "the isotropic limit". The jetty events corresponds, in the literature, to high transverse momentum p_T jets with a pencil-like emission structure in hard QCD processes. Meanwhile, the isotropic events are related to a large number of soft events associated to a low momentum transfer, and a consequence, it forms an isotropic emission of the final state of the particles (hadrons) [53].

Spherocity These novel event shape variable was proposed in [54] and studied later, see [55]. The spherocity S_0 is defined in terms of a unit vector $\hat{n}_s$ that minimizes the ratio [55, 56],

$$S_0 = \frac{\pi^2}{4} \min_{\hat{n}_s} \left(\frac{\sum_i |\vec{p}_{T,i} \times \hat{n}_s|}{\sum_i p_{T,i}} \right)^2 \tag{8}$$

Similarly to sphericity case, the values of the spherocity range from 0 to 1, because of this shape event variable is normalized by the constant $\pi^2/4$. And one can classify these values in jetty and isotropic cases as before with the same meaning, this information is supported by proton-proton collisions performed at ALICE facility [57].

Centrality For the purpose of this project, the criteria we followed for split the values of sphericity and spherocity into central, mid-central, and peripheral events are depicted in Table 1

Event splitting Criteria		
Type of events	**Impact Parameter [fm]**	**Centrality %**
Central	$b \in (0, 3.54)$	0-10%
Mid-Central	$b \in (5.04, 8.01)$	20-50%
Peripheral	$b \in (8.01, 16)$	50-100%

Table 1: This is the criteria followed to split spherocity and sphericity values into central, mid-central, and peripheral events

4 Results

The production of data corresponds to minimum bias simulations of Bi-Bi collisions at 9.2 GeV in the center-of-mass frame, those events were produced by the UrQMD event generator. The results were obtained through the analysis of 230,000 events with a impact parameter range from 0 to 16 fm. Furthermore, we selected the values for our observables within a range of pseudo-rapidity $|\eta| < 1.3$ where the Time Projection Chamber (TPC) is available to detect particles. The principal observables before selecting the range of pseudo-rapidity were the multiplicity, energy, transversal momentum , and pseudo-rapidity versus the impact parameter denoted as dN/db,

dN/dE, dN/dp_T, and $dN/d\eta$. The plots associated to the previous requirements are shown in the Fig. 2.

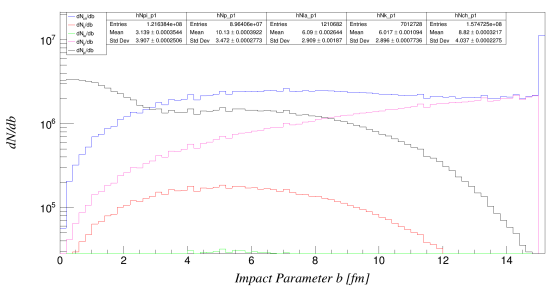

(a) No. of particles vs the impact parameter.

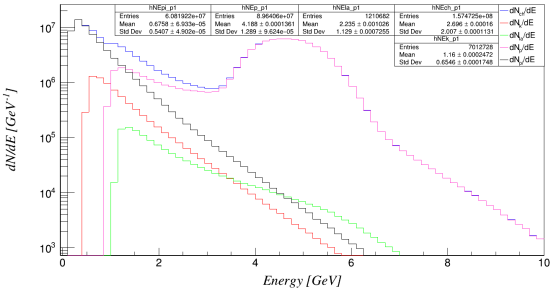

(b) Number of particles vs energy

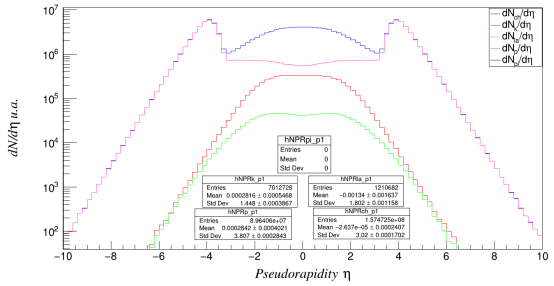

(c) No. of particles vs pseudo-rapidity

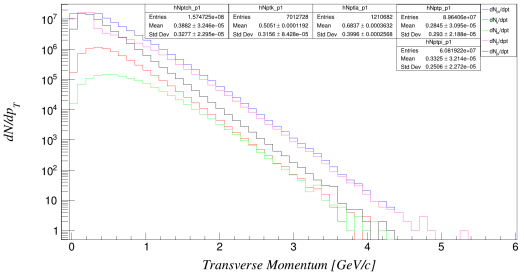

(d) Number of particles vs transverse

Figure 2: Number of particles produced in the collision versus the energy, transverse momentum, impact parameter, and pseudo-rapidity.

In the plot shown in the Fig. 2c one can notice a large quantity of protons in the vecinity of $|\eta| = 4$, this happens because of the partons involved in the collisions are taken as spectators, see 10a. That is, the protons do not interact to each other and pass through with a large amount of longitudinal momentum, this is another reason about we used the cuts in pseudo-rapidity. Subsequently, removing the particles that fall within $|\eta| > 1.3$, and calculating the mean values for each the most important observables our purposes (transversal momentum and multiplicity) are depicted in Fig. 3. In the Fig. 3a we see that most of the charged particles have a mean trans-

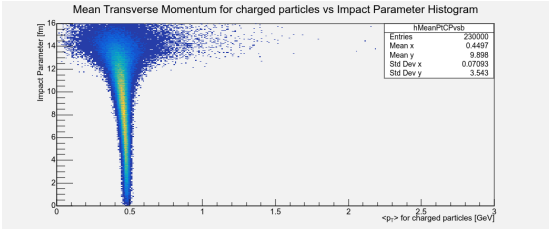

(a) $< p_T >_{CP}$ versus impact parameter

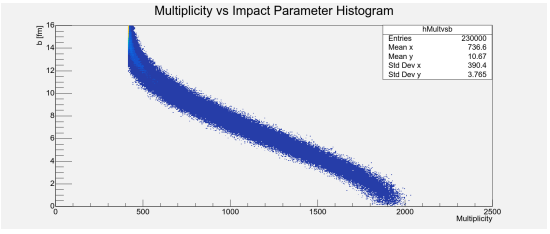

(b) Multiplicity versus impact parameter

Figure 3: Mean for transversal momentum and multiplicity after the cutting in $|\eta| > 1.3$

verse momentum (around 0.5 GeV) with a impact parameter range within 6 and

10 fm; as we will see later, this range corresponds to peripheral events. The next step was dedicated to calculate the event shape variables (ESV) by virtue of the expressions in (5) and (6), and (8) for sphericity and spherocity, respectively. The plots regarding the event shape variables are depicted in the Fig. 4a and Fig. 4b, a figure where we put them together is shown in Fig 4c. Finally, comparing these variables against the impact parameter, we obtained the following charts, see Fig. 5.

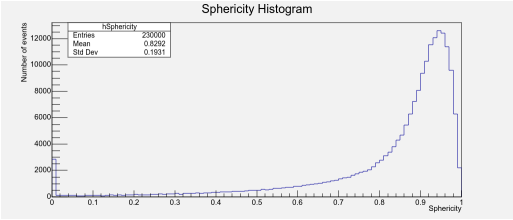

(a) Sphericity vs number of events

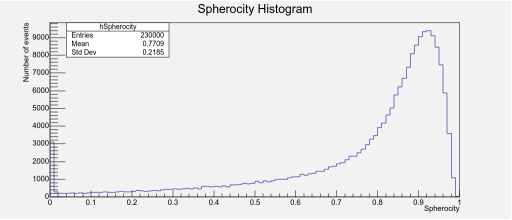

(b) Spherocity vs number of events

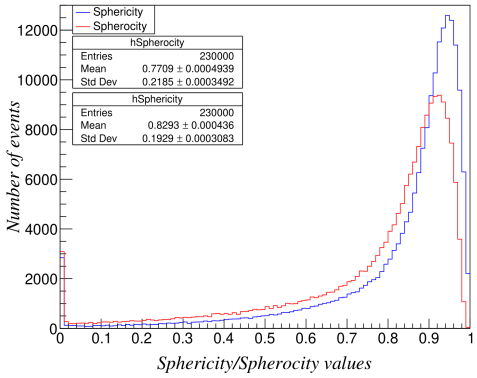

(c) Spherocity vs number of events

Figure 4: Event Shape Variables versus number of events

In the Fig. 4c the values of sphericity and spherocity are contrasted one each other in order see their behavior clearly. One can observe a certain tendency for values in both shape variables, where they are greater than 0.8, which means that most of the events have particles that propagates in an similar way in all directions, that is, the particles detected have no a preferred direction and their seems to propagate like a gas, see Fig.10b. In the same way, one can argue that it is less probable to such events propagate with a preferred direction, like a fluid. Now, we considered important to notice how the sphericity and spherocity is distributed in terms of the impact parameter, in order to know what the kind of process they came from, and the results obtained are depicted in Fig. 5. Those charts show the existence of a certain range in the impact parameter where the highest values of the sphericity and spherocity are placed, the range mentioned goes from 0.6 fm to 12 fm, where most of the points are colored in yellow. That is, in the nucleon-nucleon collision the centers are not aligned and the particles produced after the collisions (most of the times) are distributed in a homogeneous way through to the detectors, which is an interesting result.

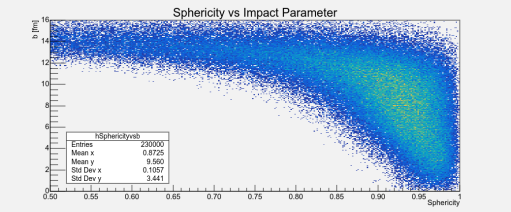

(a) Sphericity vs Impact parameter

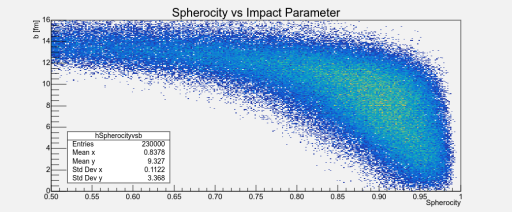

(b) sphericity and spherocity together.

Figure 5: Event Shape Variables versus Impact Parameter

As a way to explore more our data, we followed the criteria depicted on the Tab. 1, and we obtained the graphs of central, mid-central, and peripheral events for sphericity, spherocity and the mean transverse momentum for charged particles ($< p_T >_{cp}$), the Fig. 6 shows these results. The first thing to notice is the number of particles for each type of event. For central events we have 11,190 events, for mid-central 34,534 events, and for peripheral 172,469 giving a total of 218,193 events, that is, 11,807 null events or approximate a 5.13% of all the events considered. The reason for the previous result came for the UrQMD generator, since in the data recollection the program said that there were empty events. Such errors did not allow to UrQMD generator to make a proper analysis, and this could be an explanation for the anomalies presented in Fig 4a and 4b, where we have a considerable amount of events with null sphericity and spherocity. The average of sphericity, spherocity, and $< p_T >_{cp}$ can be summarized through the Tab. 2. Observing the table we can notice that as the centrality decreases, the values of spherocity and sphericity also decreases, but we still obtaining high values in event shapes for peripheral events as one could expect.

Mean values for sphericity, spherocity, and $< p_T >_{cp}$			
Type of event	**Sphericity**	**Spherocity**	$< p_T >_{cp}$ $[GeV]$
Total	0.8292 ± 0.0004366	0.7709 ± 0.0004939	0.4497 ± 0.0001603
Central	0.9618 ± 0.0001908	0.9444 ± 0.0002417	0.4796 ± 0.000113
Mid-Central	0.9345 ± 0.0001781	0.9078 ± 0.0002249	$0.4678 \pm 8.762 \times 10^{-5}$
Peripheral	0.84 ± 0.0003169	0.7971 ± 0.0003366	$0.4406 \pm 2.205 \times 10^{-4}$

Table 2: These are the ranges according to sphericity for central, mid-central, and peripheral events

Concerning on the obtaining of more information about what is happening in the collisions it is required to find the values of sphericity and spherocity by identifying the jetty and isotropic limits. By virtue of this, we first divided the number of events, at Fig 4a and Fig. 4b, in small intervals of equal size known as bins. Therefore, for the range of the jetty limit we calculated the integral up to the 20% of the total of events, once we have identified the upper limit within this range we calculated its value for each upper end obtained before, both the sphericity and spherocity. In a similar way we obtained the lowest end for the range regarding isotropic events, the difference here is the calculation of the integral, which was done up to the 80% of the events instead 20%, and obtaining its value for each event shape variable as well.

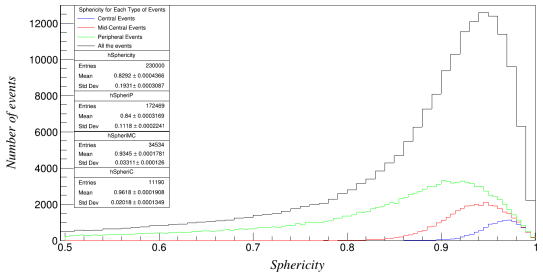

(a) Sphericity for central, mid central, and peripheral events.

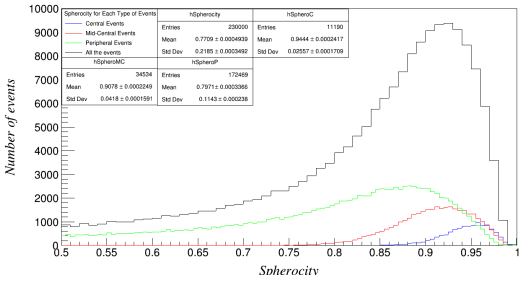

(b) Spherocity for central, mid central, and peripheral events.

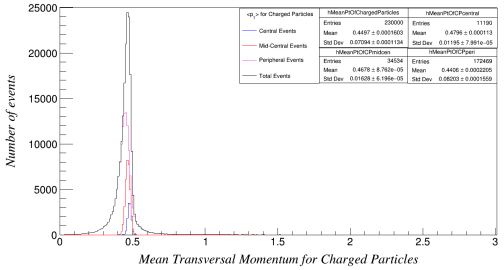

(c) $< p_T >_{cp}$ for central, mid central, and peripheral events.

Figure 6: Event Shape Variables for each type of centrality events

The ranges obtained for the previous process is depicted in Table 3 for sphericity, and Table 4 for spherocity.

Ranges for jetty and isotropic Events for Spherocity		
Type of event	**Range for Jetty events**	**Range for Isotropic events**
Central	$(0, 0.9425)$	$(0.9725, 1)$
Mid-Central	$(0, 0.9025)$	$(0.9525, 1)$
Peripheral	$(0, 0.7475)$	$(0.9125, 1)$

Table 3: These are the ranges according to sphericity for central, mid-central, and peripheral events

Ranges for jetty and isotropic Events for Spherocity		
Type of event	**Range for Jetty events**	**Range for Isotropic events**
Central	$(0, 0.9175)$	$(0.9625, 1)$
Mid-Central	$(0, 0.8675)$	$(0.9425, 1)$
Peripheral	$(0, 0.6925)$	$(0.8725, 1)$

Table 4: These are the ranges according to spherocity for central, mid-central, and peripheral events

Once we got the previous ranges we need to split multiplicity and mean transverse momentum of charged particles into sphericity (central, mid-central, and peripheral)

and spherocity (central, mid-central, and peripheral) for jetty and isotropic limits. The graphs about what we established before are in Fig. 7, Fig. 8, and Fig. 9 for multiplicity vs b, $< p_T >_{CP}$ vs b, and multiplicity vs $< p_T >_{CP}$, respectively.

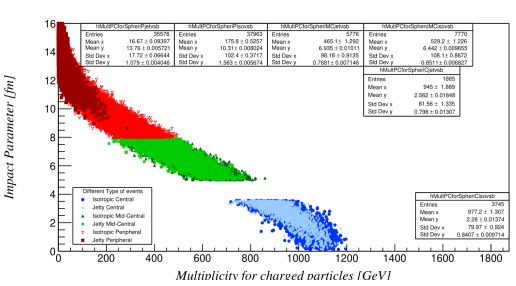

(a) Multiplicity vs b, by sphericity splitting respect to each type of centrality.

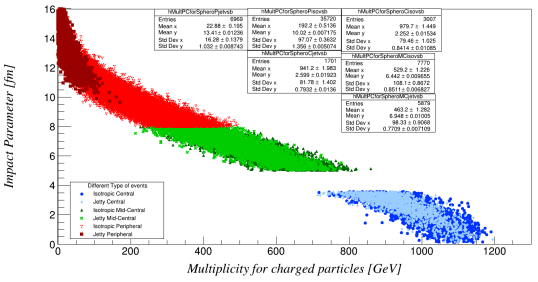

(b) Multiplicity vs b, by spherocity splitting respect to each type of centrality.

Figure 7: This figures express the dependence of multiplicity versus impact parameter respect to jetty and isotropic events for each type of centrality of sphericity and spherocity.

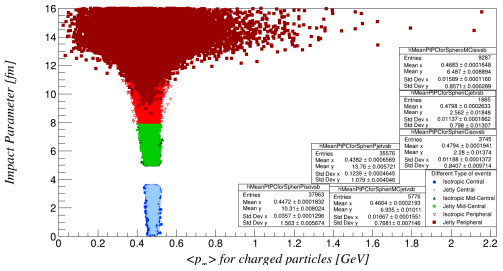

(a) $< p_T >_{CP}$ vs b, by sphericity splitting respect to each type of centrality.

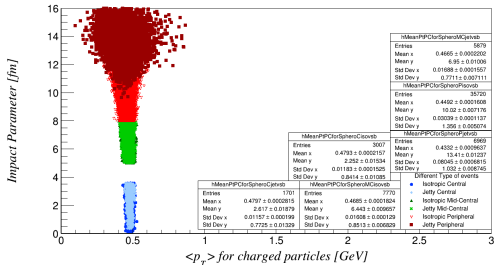

(b) $< p_T >_{CP}$ vs b, by spherocity splitting respect to each type of centrality.

Figure 8: This figures express the dependence of $< p_T >_{CP}$ vs b respect to jetty and isotropic events for each type of centrality for sphericity and spherocity.

As one can see in both graphs at Fig. 7, we found a gap in the values of the impact parameter from 3.54 fm to 5.04 fm, such a gap corresponds to the values of centrality we are not considering. In addition, we found that all the cuts in sphericity about its centrality, for jetty and isotropic splitting, one can restore a similar profile depicted in Fig 3b, we said similar on the grounds of the impact parameter gap. The information we obtain here is that most of the particles fall into isotropic central events with a mean value of 977.2±1.307 particles and 979.27± 1.449 particles for sphericity and spherocity, respectively. Besides, this events are within an impact parameter range, from 0 fm to 3.54 fm. But, if we look the case of jetty events for central sphericity and spherocity one gets 945 ± 1.889 and 941.2 ± 1.983, particles within this behavior, this describes nucleon-nucleon collision with small impact parameter where the outgoing particles follow a pen-like geometry, causing jets, which is interesting. Furthermore, in the case of isotropic peripheral sphericity events we got 175.8±0.5257, while for jetty peripheral we got 16.67±0.0939

particles, both regarding sphericity case. Equally important, we obtained a mean of 192.2 ± 0.52136 particles for isotropic and 22.88 ± 0.195 particles for jetty, both in the central spherocity regime. The graphs in Fig. 8 depict how the $< p_T >_{CP}$ is distributed versus the impact parameter both spherocity and sphericity; in addition, one can observe that the profile shown here almost replicate the behavior presented in Fig 3a. Finally, the chart in Fig. 9 shows that most of the charged particles produced fall within a range of values from $0.4382 \pm 6.569 \times 10^{-4}$ to $0.4798 \pm 2.633 \times 10^{-4}$ GeV in sphericity splitting, and from $0.4332 \pm 9.63 \times 10^{-4}$ to $0.4796 \pm 2.746 \times^{-4}$ GeV where the lowest values for each type of centrality corresponds to jetty events, and the highest values to isotropic events, in both sphericity and spherocity splitting.

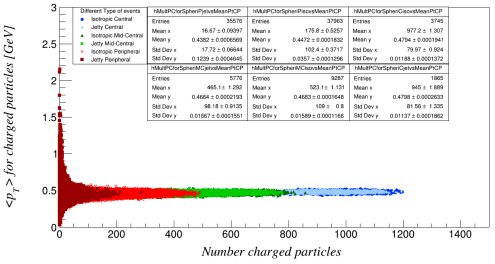

(a) Multiplicity vs $< p_T >_{CP}$, by sphericity splitting respect to each type of centrality.

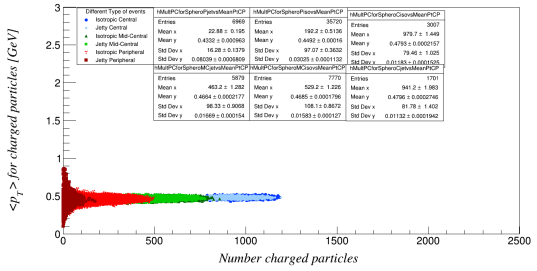

(b) Multiplicity vs $< p_T >_{CP}$, by spherocity splitting respect to each type of centrality.

Figure 9: This figures express the dependence of multiplicity vs $< p_T >_{CP}$ respect to jetty and isotropic events for each type of centrality for sphericity and spherocity.

5 Conclusions

Through these weeks of data analysis we found five main insights. First, the picks around $|\eta| = 4$ in the proton multiplicity versus pseudo-rapidity Fig. 2c, $dN_{ch}/d\eta$. There, we found that these values can alter our analysis since they corresponds to those nucleons that do not collide and pass throuh the Fast Forwar Detector, in view of that fact, this particles carry a important amount of longitudinal momentum, which can alter our results in following considerations. So, we opted for throw pseudo-rapidity higher 1.3 away. Second, we noticed the grand amount of sphericity and spherocity values surrounding 0.9 in Fig 4c, comparing the versus the impact parameter we found that most of the values are related to a certain range of impact parameter, but this information is not enough to make conclusions. As a parenthesis we observed certain anomalies in the charts regarding event shape variables 4c. The reason the number of null events due to errors presented in the data collection, where the 5.13% are empty events where we did not exclude, and the effect is shown there. Bringing the discussion regarding shape variables back, we found in the jetty and isotropic splitting for mean transverse momentum and multiplicity for charged particles a way to characterize the shape of the resulting particles when they are traveling to the detectors, but we obtained some questionable result, such as the large number of particles with a isotropic distribution coming from a peripheral event,

since one could expect that this type of collisions produce more jetty events that isotropic. This consequence suggests that we have no enough information about what is going on during the process. Therefore, we need more event shape variables to take in account in order to have solid argument and, hence, make strong conclusions about the dynamics of this process. In addition, we ignored other effects, such as vortical and magnetic. Further study about event shape variables is pictured in future, meanwhile, we can argue that sphericity and spherocity are useful variables in order to separate different type of events, but they have limitations and we need combine them with others.

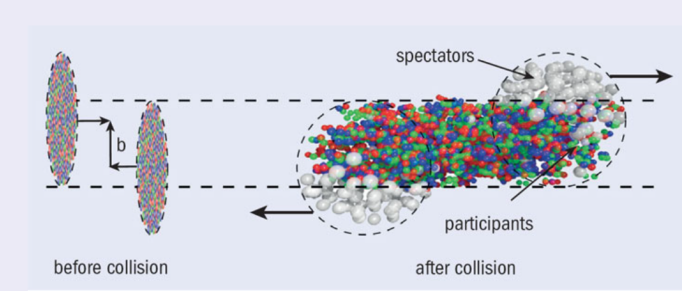

(a) Two heavy ion are shown before and after the collision with an impact parameter. Image taken from http://bit.ly/42X8rRm.

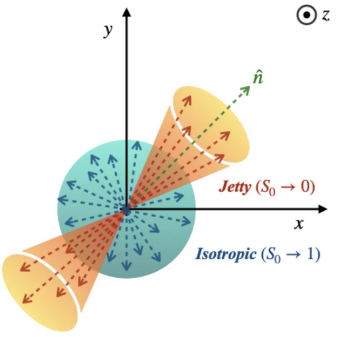

(b) Representation for jetty and isotropic events, using spherocity as ESV [58].

Figure 10: Schematic representations for heavy ion collisions before and after the process, and a representation for jetty and isotropic event using spherocity as event shape variable (ESV)

Acknowledgments

I acknowledge Dr. I. Maldonado for her support about software problems and out-of-class discussions a through Interest Wave 8. In addition, I am grateful to Dr. L. A. Hernández for help in the theoretical discussion regarding Quantum Cromo Dynamics phase diagram and all the references he gave me in order to broadening my perspective. Finally, I acknowledge to Nishant Guarav for his support and teamwork through Interest Wave 8.

References

[1] D. Griffiths, *Introduction to elementary particles* (2008).

[2] M. Gell-Mann, Physics Letters **8**, 214–215 (1964).

[3] G. Zweig, "An SU(3) model for strong interaction symmetry and its breaking. Version 1", (1964).

[4] E. D. Bloom, D. H. Coward, H. DeStaebler, J. Drees, G. Miller, L. W. Mo, R. E. Taylor, M. Breidenbach, J. I. Friedman, G. C. Hartmann, and H. W. Kendall, Phys. Rev. Lett. **23**, 930–934 (1969).

[5] M. Breidenbach, J. I. Friedman, H. W. Kendall, E. D. Bloom, D. H. Coward, H. DeStaebler, J. Drees, L. W. Mo, and R. E. Taylor, Phys. Rev. Lett. **23**, 935–939 (1969).

[6] S. W. Herb, D. C. Hom, L. M. Lederman, J. C. Sens, H. D. Snyder, J. K. Yoh, J. A. Appel, B. C. Brown, C. N. Brown, W. R. Innes, K. Ueno, T. Yamanouchi, A. S. Ito, H. Jöstlein, D. M. Kaplan, and R. D. Kephart, Phys. Rev. Lett. **39**, 252–255 (1977).

[7] R. P. Feynman, Phys. Rev. Lett. **23**, 1415–1417 (1969).

[8] Nature **548**, 62–65 (2017).

[9] G. Aad et al. (ATLAS), Eur. Phys. J. C **72**, 2211 (2012).

[10] B. Abelev et al. (ALICE), Eur. Phys. J. C **72**, 2124 (2012).

[11] S. A. Bass, M. Belkacem, M. Bleicher, M. Brandstetter, L. V. Bravina, C. Ernst, L. Gerland, M. Hofmann, S. Hofmann, J. Konopka, G. Mao, L. W. Neise, S. Soff, C. Spieles, H. J. Weber, L. A. Winckelmann, H. Stocker, W. Greiner, C. Hartnack, J. Aichelin, and N. S. Amelin, Progress in Particle and Nuclear Physics **41**, 255–369 (1998).

[12] M. Bleicher, E. E. Zabrodin, C. Spieles, S. A. Bass, C. Ernst, S. Soff, L. V. Bravina, M. Belkacem, H. J. Weber, H. Stocker, and W. Greiner, Journal of Physics G **25**, 1859–1896 (1999).

[13] V. Abgaryan et al. (MPD), Eur. Phys. J. A **58**, 140 (2022).

[14] A. Bazavov, H.-T. Ding, P. Hegde, O. Kaczmarek, F. Karsch, N. Karthik, E. Laermann, A. Lahiri, R. Larsen, S.-T. Li, S. Mukherjee, H. Ohno, P. Petreczky, H. Sandmeyer, C. Schmidt, S. Sharma, and P. Steinbrecher, Physics Letters B **795**, 15–21 (2019).

[15] Y. Aoki, G. Endrődi, Z. Fodor, S. D. Katz, and K. K. Szabó, Nature **443**, 675–678 (2006).

[16] A. Ayala, L. A. Hernández, M. Loewe, J. C. Rojas, and R. Zamora, The European Physical Journal A **56**, 10.1140/epja/s10050-020-00086-z (2020).

[17] M. Asakawa and K. Yazaki, Nucl. Phys. A **504**, 668–684 (1989).

[18] A. Ayala, A. Bashir, J. Cobos-Martınez, S. Hernández-Ortiz, and A. Raya, Nuclear Physics B **897**, 77–86 (2015).

[19]A. Ayala, S. Hernandez-Ortiz, and L. A. Hernandez, Rev. Mex. Fis. **64**, 302–313 (2018).

[20]M. A. Stephanov, PoS **LAT2006**, edited by T. Blum, M. Creutz, C. DeTar, F. Karsch, A. Kronfeld, C. Morningstar, D. Richards, J. Shigemitsu, and D. Toussaint, 024 (2006).

[21]J. Randrup and J. Cleymans, Phys. Rev. C **74**, 047901 (2006).

[22]S. Blacker, N.-U. F. Bastian, A. Bauswein, D. B. Blaschke, T. Fischer, M. Oertel, T. Soultanis, and S. Typel, Phys. Rev. D **102**, 123023 (2020).

[23]E. Most, L. Papenfort, V. Dexheimer, M. Hanauske, H. Stoecker, and L. Rezzolla, The European Physical Journal A **56**, 10.1140/epja/s10050-020-00073-4 (2020).

[24]T. Klähn, D. Blaschke, and F. Weber, Physics of Particles and Nuclei Letters **9**, 484–487 (2012).

[25]D. Blaschke, D. E. Alvarez-Castillo, and S. Benic, PoS **CPOD2013**, 063 (2013).

[26]A. Bauswein, N.-U. F. Bastian, D. B. Blaschke, K. Chatziioannou, J. A. Clark, T. Fischer, and M. Oertel, Phys. Rev. Lett. **122**, 061102 (2019).

[27]O. V. Rogachevsky, A. S. Sorin, and O. V. Teryaev, Phys. Rev. C **82**, 054910 (2010).

[28]Y. B. Ivanov and A. A. Soldatov, Phys. Rev. C **97**, 044915 (2018).

[29]A. Ayala et al., Phys. Lett. B **810**, 135818 (2020).

[30]A. Ayala, I. Domınguez, I. Maldonado, and M. E. Tejeda-Yeomans, Phys. Rev. C **105**, 034907 (2022).

[31]V. Skokov, A. Y. Illarionov, and V. Toneev, Int. J. Mod. Phys. A **24**, 5925–5932 (2009).

[32]A. N. Tawfik, Indian J. Phys. **91**, 93–99 (2017).

[33]M. Alford, K. Rajagopal, and F. Wilczek, Physics Letters B **422**, 247–256 (1998).

[34]R. Rapp, T. Schäfer, E. Shuryak, and M. Velkovsky, Physical Review Letters **81**, 53–56 (1998).

[35]J. Berges and K. Rajagopal, Nuclear Physics B **538**, 215–232 (1999).

[36]T. Hatsuda, M. Tachibana, N. Yamamoto, and G. Baym, Phys. Rev. Lett. **97**, 122001 (2006).

[37]D. Blaschke, G. Röpke, Y. Ivanov, M. Kozhevnikova, and S. Liebing, Springer Proc. Phys. **250**, edited by D. Elia, G. E. Bruno, P. Colangelo, and L. Cosmai, 183–190 (2020).

[38]J. Mohs, M. Ege, H. Elfner, and M. Mayer, Phys. Rev. C **105**, 034906 (2022).

[39]P. Napolitani, M. Colonna, F. Gulminelli, E. Galichet, S. Piantelli, G. Verde, and E. Vient, Phys. Rev. C **81**, 044619 (2010).

[40]Brandt, Bastian B., Endr"odi, Gergely, and Schmalzbauer, Sebastian, EPJ Web Conf. **175**, 07020 (2018).

[41]A. B. Migdal, Rev. Mod. Phys. **50**, 107–172 (1978).

[42]V. Ruck, M. Gyulassy, and W. Greiner, Z. Phys. A **277**, 391–394 (1976).

[43]T. Khunjua, K. Klimenko, and R. Zhokhov, Symmetry **11**, 10.3390/sym11060778 (2019).

[44]T. U. group, *The urqmd user guide*, English, version Version 3.4, Frankfurt Institute for Advanced Studies (), 48 pp., November 16, 2011.

[45]C. Wong, Introduction to High-energy Heavy-ion Collisions (World Scientific, 1994).

[46]A. Ortiz, "Experimental results on event shapes at hadron colliders", in *Multiple parton interactions at the LHC* (WORLD SCIENTIFIC, Nov. 2018), pp. 343–357.

[47]A. Banfi, G. P. Salam, and G. Zanderighi, "Resummed event shapes at hadron - hadron colliders", JHEP **08**, 062 (2004).

[48]X.-N. Wang and M. Gyulassy, Phys. Rev. D **44**, 3501–3516 (1991).

[49]M. Gyulassy, K. Frankel, and H. Stöcker, Physics Letters B **110**, 185–188 (1982).

[50]J. Randrup, Computer Physics Communications **77**, 153–166 (1993).

[51]P. Danielewicz and M. Gyulassy, Physics Letters B **129**, 283–288 (1983).

[52]J. Bondorf, C. Dasso, R. Donangelo, and G. Pollarolo, Physics Letters B **240**, 28–32 (1990).

[53]S. Sarkar, P. Mali, and A. Mukhopadhyay, Eur. Phys. J. A **58**, 139 (2022).

[54]A. Banfi, G. P. Salam, and G. Zanderighi, Journal of High Energy Physics **2010**, 10.1007/jhep06(2010)038 (2010).

[55]A. Ortiz, G. Paić, and E. Cuautle, Nucl. Phys. A **941**, 78–86 (2015).

[56]E. Cuautle, R. Jimenez, I. Maldonado, A. Ortiz, G. Paic, and E. Perez, (2014).

[57]S. Acharya et al. (ALICE), Eur. Phys. J. C **79**, 857 (2019).

[58]S. Prasad, N. Mallick, D. Behera, R. Sahoo, and S. Tripathy, Scientific Reports **12**, 10.1038/s41598-022-07547-z (2022).